

Supporting Information

High performance ferrite nanoparticles through nonaqueous redox phase tuning

Ritchie Chen^{1,2}, Michael G. Christiansen^{1,2}, Alexandra Sourakov¹, Alan Mohr³, Yuri Matsumoto⁴, Satoshi Okada⁴, Alan Jasanoff^{4,5,6}, Polina Anikeeva^{1,2*}

¹Department of Materials Science and Engineering, Massachusetts Institute of Technology, Cambridge, MA 02139. ²Research Laboratory of Electronics, Massachusetts Institute of Technology, Cambridge, MA 02139.

³Department of Chemical Engineering, Massachusetts Institute of Technology, Cambridge, MA 02139.

⁴Department of Biological Engineering, Massachusetts Institute of Technology, Cambridge, MA 02139.

⁵Department of Brain & Cognitive Sciences, Massachusetts Institute of Technology, Cambridge, MA 02139.

⁶Department of Nuclear Science & Engineering, Massachusetts Institute of Technology, Cambridge, MA 02139.

*corresponding author: anikeeva@mit.edu

Materials and Methods.

Sodium oleate (95%, TCI America) and iron chloride hexahydrate (99%+, Acros) were purchased from different vendors. All other solvents and reagents were purchased from Sigma-Aldrich: oleic acid (90%), octadecane (99%), 1-octadecene (90%), squalene (99%), dibenzyl ether (98%), dioctyl ether (99%), trimethylamine N-oxide (98%), poly(maleic anhydride-alt-1-octadecene) ($M_n=30,000-50,000$), and poly(ethylene glycol) methyl ether ($M_n=5000$).

Synthesis of metal-oleate complex. In a 1 L 3 neck flask, 30 mmol of $\text{FeCl}_3 \cdot 6\text{H}_2\text{O}$ and 92 mmol of sodium oleate was heated to reflux (60 °C) in a solvent mixture comprised of 200 mL of hexane, 100 mL of ethanol, and 100 mL of ddH₂O for one hour under N₂. The hexane layer containing the iron-oleate complex was then extracted with a separatory funnel and washed twice with ddH₂O. The iron-oleate mixture was heated to 110 °C in a beaker and dried overnight stirring on a hotplate.

Synthesis of magnetic nanoparticles with different solvents. In a 250 mL 3 neck flask, 5 mmol of iron-oleate, 2.5 mmol of oleic acid, and 20 mL of solvent (octadecane, 1-octadecene, squalene, dioctyl ether, or dibenzyl ether) was degassed at 90 °C for 30 minutes. Then the mixture was heated to 200°C under N₂, then to reflux at 3.3 °C/min and held at the reflux temperature for 30 minutes. The nanoparticles were extracted by transferring the reaction solution into 50 mL conical tubes, adding 30 mL of ethanol to promote flocculation, then precipitated by centrifuging at 10,000 rpm for 10 minutes. Following two washes (disperse in hexane followed by the addition of ethanol then centrifugation), the nanoparticle pellet was re-dispersed in 10 mL of chloroform.

Synthesis of magnetic nanoparticles using SORT. In a 250 mL 3 neck flask, 5 mmol of iron-oleate and 5 mmol (10 nm), 10 mmol (15 nm), 12.5 mmol (19 nm), or 15 mmol (27 nm) of oleic acid was combined in a 2:1 volume ratio of 1-octadecene (10 mL) and dibenzyl ether (5 mL) and degassed at 90 °C for 30 minutes. Then the mixture was heated to 200°C under N₂, then to reflux (325 °C) at 3.3 °C/min and held at the reflux temperature for 30 minutes. After pelleting and washing, the nanoparticle pellet was re-dispersed in 5 mL of chloroform.

Oxidation of as-synthesized nanoparticles. After cooling the reaction solution to room temperature, 15 mmol of trimethylamine N-oxide was added, heated to 140 °C in air, and allowed to react for 30 minutes.

FTIR. Aliquoted reactions collected at different time points were diluted 1:10 in chloroform. 10 μ L of this solution was drop-casted then sandwiched between NaCl windows (International Crystal Laboratories). FTIR spectra was collected on a Thermo Fisher FTIR6700 Spectrometer using transmission mode. Aliquots during the course of a reaction were drawn using a 1 mL gas-tight Hamilton syringe.

Structural and magnetic characterization. Powder x-ray diffraction patterns of as-synthesized nanoparticles was collected on a three-circle diffractometer coupled to a Bruker-AXS Smart Apex charged-coupled-device (CCD) detector with graphite-monochromated Mo K α radiation ($\lambda = 0.71073 \text{ \AA}$). Field-cooled (5T) hysteresis curves at 5 K were measured using a superconducting quantum interference device (SQUID, MPMS-XL, Quantum Design). SQUID temperature dependent magnetization curves were measured with an applied field of 10 mT. Room temperature hysteresis curves were generated on a vibrating sample magnetometer (VSM, Digital Measurement Systems Model 880A).

Phase transfer and PEGylation. 100 μ L of nanoparticle solution dispersed in chloroform (~ 10 mg/mL) was combined with 1 mL of poly(ethylene glycol) grafted poly(maleic anhydride-alt-1-octadecene) solution (10 mg/mL in chloroform) and sonicated for 15 minutes. After evaporating the chloroform under vacuum, 2 mL of 1X Tris/Borate/EDTA buffer was added and sonicated for 30 minutes. The nanoparticles were magnetic separated and washed twice with water, then reconstituted in 1 mL of water (~ 1 mg/mL) and sonicated for 10 minutes.

Elemental Analysis. Nanoparticles were digested in 37% v/v HCl overnight at 60 °C and diluted in 2 wt% HNO₃. Inductively coupled plasmon emission spectroscopy (ICP-ES, Jobin-Yvon Ultima-C) was used to quantify the elemental concentration.

SLP measurements. PEG-coated MNPs were adjusted to 2 mg/mL prior to SLP measurements. A custom-built series resonant circuit powered by a 200 W amplifier (1020L, Electronics & Innovation) was used to generate alternating AMF, with the field amplitude measured with a

pickup coil and oscilloscope. Temperature measurements were made with a fiber optic temperature probe (Omega HHTFO-101).

MR Imaging. MRI experiments were performed on a 7 T PharmaScan[®] MRI instrument (Bruker). The relaxivity of the samples were determined by using the MSME (multi-slice multi-echo) sequence at room temperature with the following: TR (repetition time) = 2 s, 30 echoes with 24 ms TE (echo time) averaged over 4 acquisitions, FOV (field of view) = 5x5 cm, matrix = 256x256, and section thickness = 2 mm.

HEK293FT Cell Experiments. HEK293FT cells were seeded on 5 mm cover glass coated with matrigel and transfected with TRPV1-p2A-mCherry and gCaMP6s using lipofectamine. Cells were placed in a 7.5 mm gap cut into a soft ferromagnetic core and immersed in 1.5 mg/mL [Fe] of nanoparticles. An AMF of $f = 150$ kHz and $H_0 = 30$ kA/m was applied while real-time fluorescence recordings of gCaMP6s was captured on an inverted microscope as previously described.¹

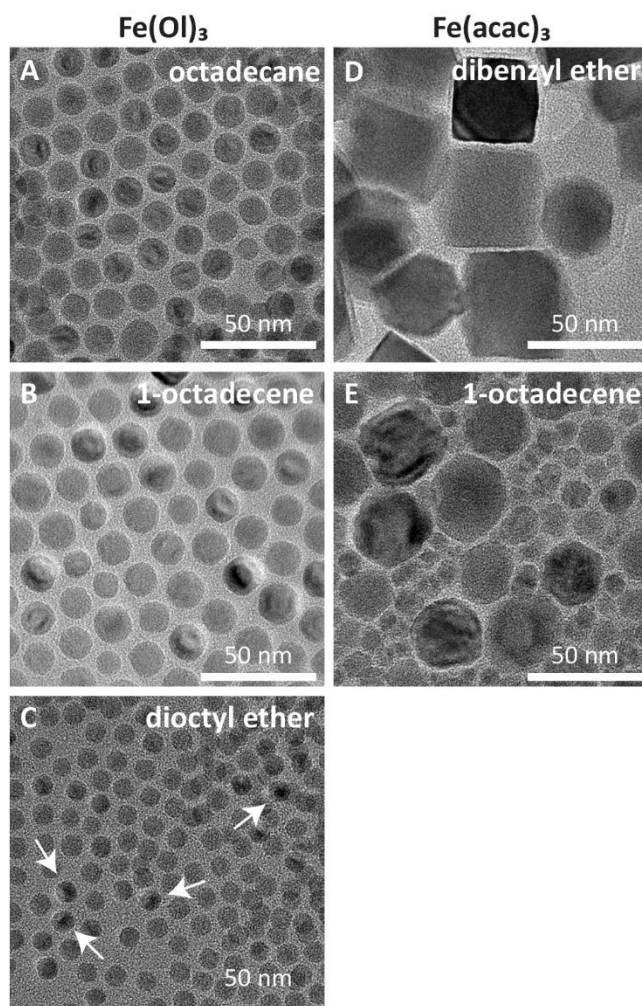


Figure S1. TEM micrographs of ferrite nanoparticles synthesized from Fe(OI)_3 (A-C) and Fe(acac)_3 (D,E) decomposition in the indicated solvent. Biphasic core-shell nanoparticles are evident based on contrast. White arrow indicates core-shell geometry even in dioctyl ether.

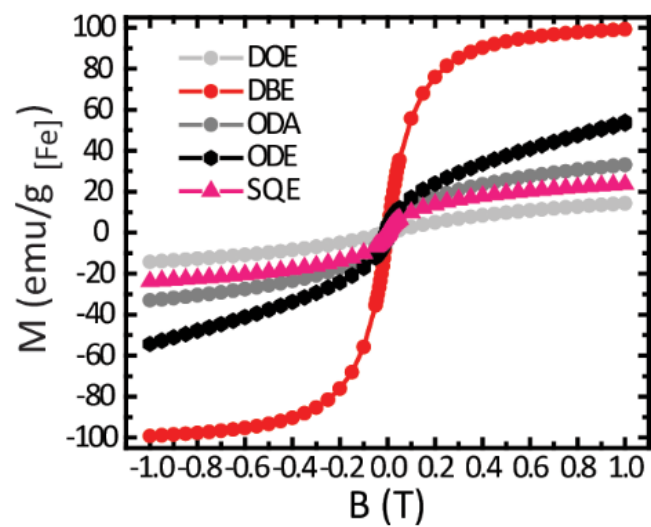


Figure S2. Room temperature magnetization curve for the various ferrite nanoparticles synthesized in different solvents: dioctyl ether (DOE), dibenzyl ether (DBE), octadecane (ODA), 1-octadecene (ODE), and squalene (SQE).

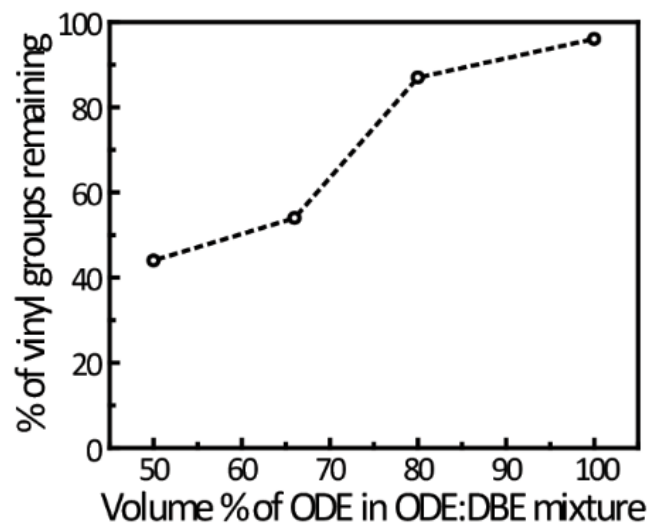


Figure S3. Integrated area of the vinyl peak of ODE ($=C-H$, 910 cm^{-1}) after 30 minutes of reflux normalized to the initial integrated area of the same peak at $200\text{ }^{\circ}\text{C}$ for different volume ratios of ODE:DBE with all other reaction parameters remaining the same.

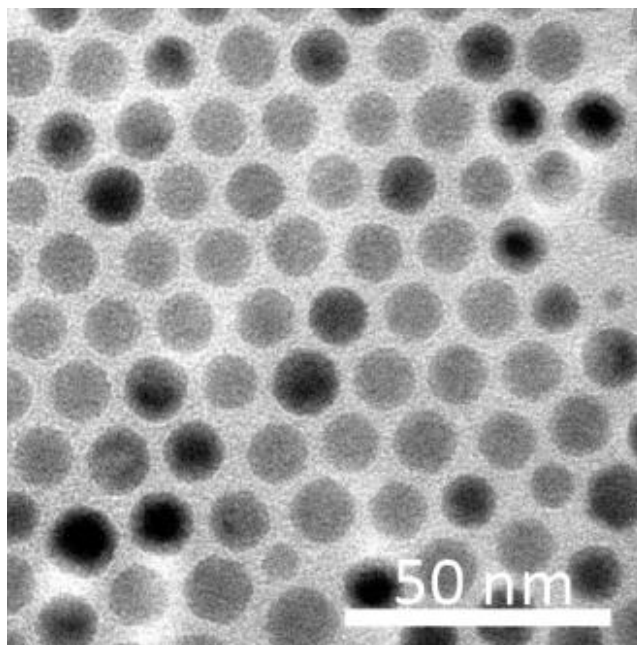


Figure S4. TEM image of nanoparticles synthesized in 15 mL of ODE with 10 mmol oleic acid and 10 mmol of benzaldehyde. Without the addition of DBE, the nanoparticles have core-shell morphology characteristic of biphasic nanoparticles, demonstrating that radicals generated during decomposition of DBE into benzaldehyde is necessary for the production of nearly-defect free nanoparticles.

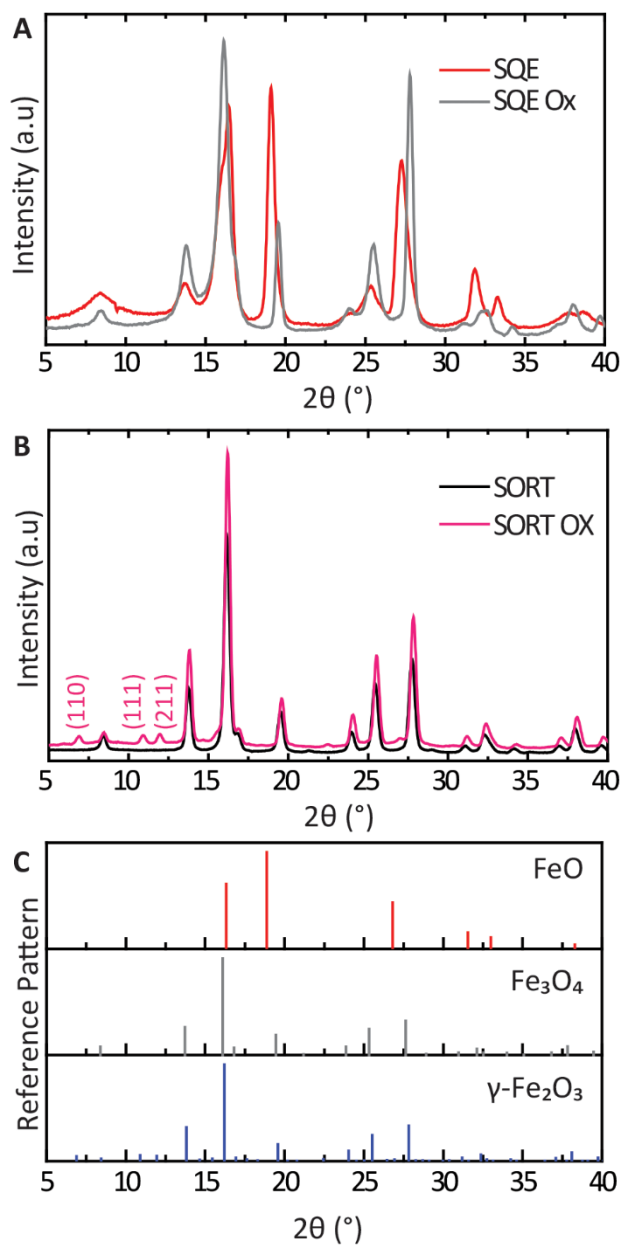


Figure S5. Powder x-ray diffractogram of (A) SQE biphasic nanoparticles (red) and SQE oxidized nanoparticles containing defects (grey), and (B) as-synthesized ferrite nanoparticles that underwent SORT (black) and SORT oxidized nanoparticles (magenta). (C) Reference pattern of wüstite (FeO), magnetite (Fe_3O_4), and maghemite ($\gamma\text{-Fe}_2\text{O}_3$).

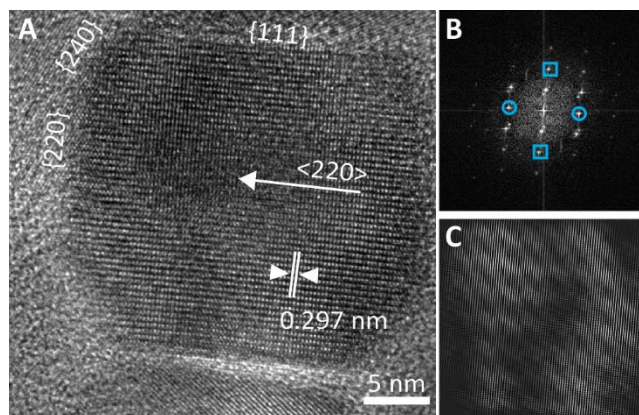


Figure S6. (A) High-resolution transmission micrograph of single nanoparticle synthesized by SORT. (B) Fast Fourier transform of the single particle image with the {111} and {220} marked \circ and \square respectively. (C) Reconstructed image exhibiting single-crystalline, inverse spinel nanoparticles free of the wüstite phase.

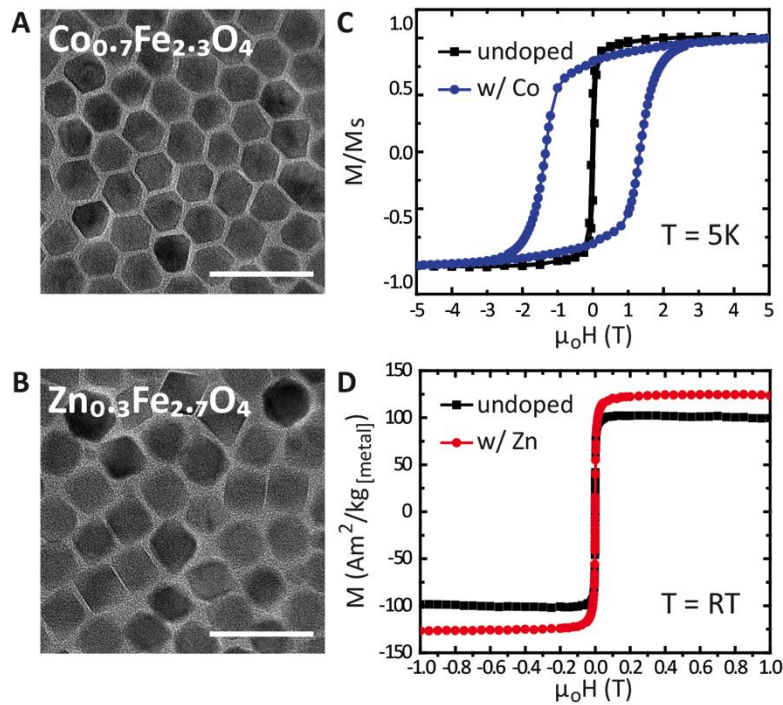


Figure S7. Doped ferrites with tunable magnetic properties. Transmission electron microscopy of (A) cobalt-doped ferrite MNPs and (B) zinc-doped ferrite MNPs. Degree of dopant incorporation was measured by ICP-AES and is indicated on the image. Scale bar = 50 nm. (C) Normalized magnetization curve measured for cobalt-doped MNPs in (A) at 5K exhibiting nearly 40 fold increase in the coercive field H_c compared to undoped iron oxide of the same size. (D) Room-temperature magnetization curve of zinc-doped MNPs in (B) showing increased saturation magnetization M_s compared to undoped iron oxide of the same size.

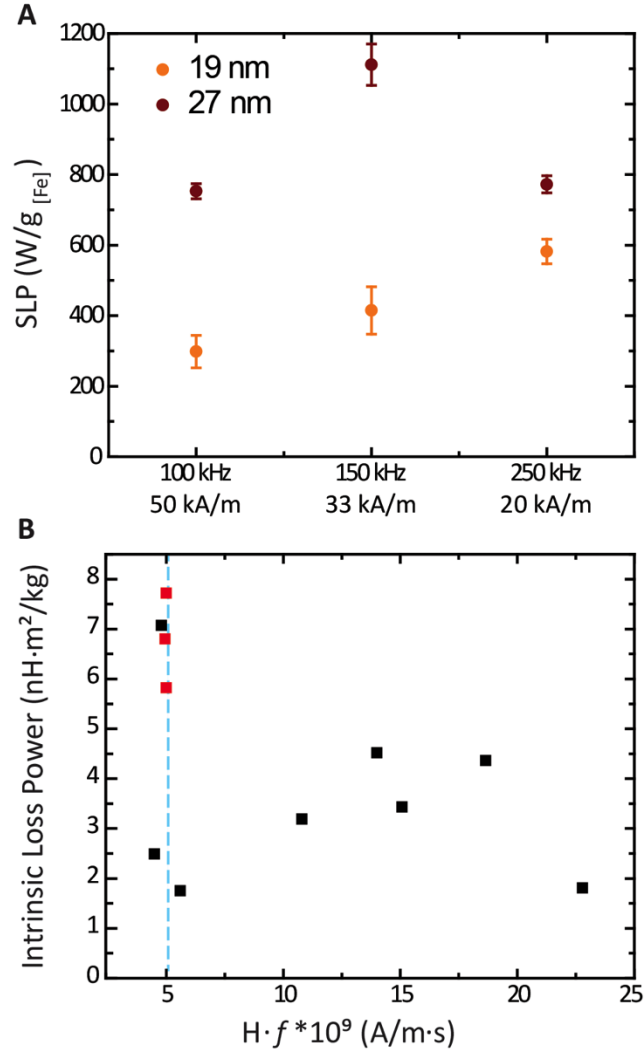


Figure S8. Specific and intrinsic loss powers of SORT nanoparticles. (A) SLP values measured for 19 and 27 nm SORT-synthesized iron oxide MNPs at different field frequencies and amplitudes with constant field product $H \cdot f = 5 \cdot 10^9$ A/m·s. (B) Intrinsic loss powers of synthetic iron oxide nanoparticles used in this study (red) compared to other reported values (black) as a function of the field product $H \cdot f$. Blue dashed line indicates upper limit set by the Brezovich criterion. Tabulated values are reported in Table S1.

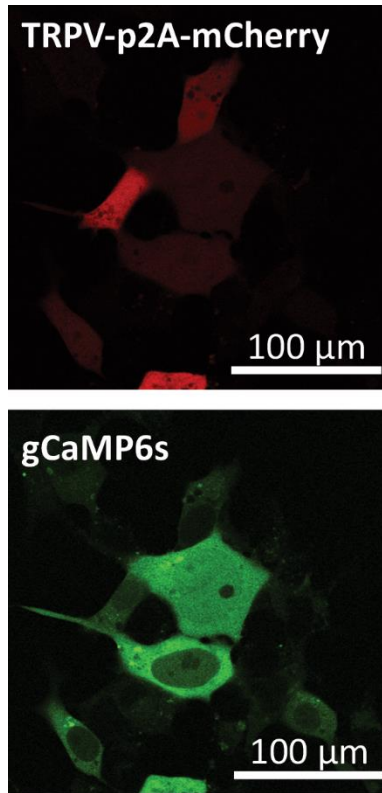


Figure S9. Fluorescence image of HEK293FT cells co-transfected with the heat-sensitive ion channel TRPV1 (red) and genetically-encoded fluorescent Ca^{2+} indicator gCaMP6s (green).

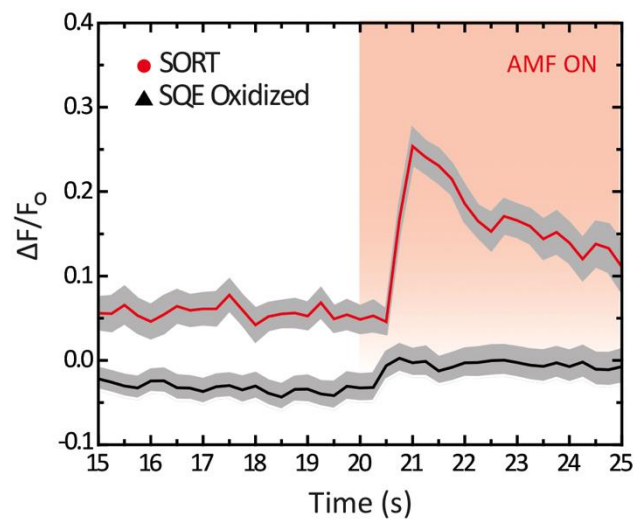


Figure S10. Close-up of Figure 5A showing minor onset within ~ 750 ms of applied field (AMF ON) for SORT synthesized nanoparticles.

Table S1. Summary of specific loss power (SLP) and intrinsic loss power (ILP) of several synthetic iron oxide nanoparticle sizes and morphologies measured at different field amplitude (H) and frequency (f).

| Size | Morphology | H (kA/m) | f (kHz) | $H \cdot f \cdot 10^9$ (A/m·s) | SLP (W/g) | ILP (nH·m ² /kg) | Reference |
|---------|------------|-------------|------------|-----------------------------------|--------------|--------------------------------|--------------|
| 10 nm | sphere | 15 | 300 | 4.5 | 168 | 2.5 | ² |
| 19 nm | cube | 15 | 320 | 4.8 | 509 | 7.07 | ³ |
| 19 nm | faceted | 20 | 250 | 5 | 582 | 5.82 | This study |
| 28 nm | faceted | 33 | 150 | 4.95 | 1111 | 6.80 | This study |
| 28 nm | faceted | 20 | 250 | 5 | 772 | 7.72 | This study |
| 43 nm | octahedral | 16 | 350 | 5.6 | 157 | 1.75 | ⁴ |
| 19 nm | sphere | 27 | 400 | 10.8 | 930 | 3.19 | ⁵ |
| 70 nm | ring | 35 | 400 | 14 | 2213 | 4.52 | ⁶ |
| 24.9 nm | multi-core | 29 | 520 | 15.08 | 1500 | 3.43 | ⁷ |
| 16 nm | core shell | 37.3 | 500 | 18.65 | 3034 | 4.36 | ⁸ |
| 43 nm | octahedral | 63.66 | 358 | 22.79 | 2629 | 1.81 | ⁴ |

References.

1. Chen, R.; Romero, G.; Christiansen, M. G.; Mohr, A.; Anikeeva, P. *Science* **2015**, 347, 1477-1480.
2. Pradhan, P.; Giri, J.; Samanta, G.; Sarma, H. D.; Mishra, K. P.; Bellare, J.; Banerjee, R.; Bahadur, D. *J. Biomed. Mater. Res. Part B Appl. Biomater* **2007**, 81B, 12-22.
3. Guardia, P.; Di Corato, R.; Lartigue, L.; Wilhelm, C.; Espinosa, A.; Garcia-Hernandez, M.; Gazeau, F.; Manna, L.; Pellegrino, T. *ACS Nano* **2012**, 6, 3080-3091.
4. Lv, Y.; Yang, Y.; Fang, J.; Zhang, H.; Peng, E.; Liu, X.; Xiao, W.; Ding, J. *RSC Advances* **2015**, 5, 76764-76771.
5. Liu, X. L.; Fan, H. M.; Yi, J. B.; Yang, Y.; Choo, E. S. G.; Xue, J. M.; Fan, D. D.; Ding, J. *J. Mater. Chem.* **2012**, 22, 8235-8244.
6. Liu, X. L.; Yang, Y.; Ng, C. T.; Zhao, L. Y.; Zhang, Y.; Bay, B. H.; Fan, H. M.; Ding, J. *Adv. Mater.* **2015**, 27, 1939-1944.
7. Lartigue, L.; Hugounenq, P.; Alloyeau, D.; Clarke, S. P.; Lévy, M.; Bacri, J.-C.; Bazzi, R.; Brougham, D. F.; Wilhelm, C.; Gazeau, F. *ACS Nano* **2012**, 6, 10935-10949.
8. Lee, J.; Jang, J.; Choi, J.; Moon, S. H.; Noh, S.; Kim, J.; Kim, J.; Kim, I.; Park, K. I.; Cheon, J. *Nature Nanotechnology* **2011**, 6, 418-422.